Available online at www.sciencedirect.com
ScienceDirect
Journal of Electrostatics 66 (2008) 1–7
Journal of ELECTROSTATICS
www.elsevier.com/locate/elstat

Coupling mechanical rotation and EHD actuation in flow past a cylinder

A. Gronskis[a,*], J. D'Adamo[a], G. Artana[b], A. Camillieri[a], J.H. Silvestrini[c]

[a] University of Buenos Aires, Argentina
[b] University of Buenos Aires and CONICET, Argentina
[c] Pontificia Universidade Catolica do Rio Grande do Sul, Brazil

Received 16 April 2007; received in revised form 4 June 2007; accepted 16 June 2007
Available online 16 July 2007

Abstract

The introduction of an electro-hydrodynamic (EHD) force in high performance numerical simulation may pose some problems as a consequence of the large differences between time or spatial scales of the physics of the discharge and those of interest for the fluid flow description. In this paper, we try to simplify this problem by looking for a correspondence between the global flow modifications produced by an EHD actuation and those by a moving body surface. Direct numerical simulations (DNS) of flow past a rotating cylinder are performed. For a flow regime corresponding to Reynolds number based on the cylinder diameter and free-stream velocity of the flow of 125 (wake-transition regime), the simulations allow us to make a comparison with particle image velocimetry (PIV) measures of the flow induced by a dielectric barrier discharge (DBD) plasma actuator suitably disposed on the cylinder surface. The results obtained from the projection of mean velocity fields show that the time-averaged vortical structures in the two cases enable us to establish a good analogy between actuations produced by both mechanisms.

Keywords: Flow control; Plasma actuators; Dielectric barrier devices; Particle image velocimetry; Direct numerical simulation; Rotating cylinder

1. Introduction

Electro-hydrodynamic (EHD) actuators for flow control with aims to improve aerodynamic design have been receiving special attention in the last years [1–3]. Through the ionization of the flowing air close to the surface of a body, EHD devices produce a modification of the condition of the flow at the wall proximity. The charged particles present in the ionized air (plasma) experience an electric force that is transmitted through particle collision to the neutrals of the flowing air. The expression of this force on the fluid depends on the discharge characteristics, and in some cases there can exist a two-way interaction created by electric forces as they elicit a mechanical response that, in turn, alters the fields. The implementation of this force in numerical flow simulations is of interest, as it could be used to optimize the design and placement of plasma actuators for different applications for flow control. Detailed studies on how to implement the electric force coupling in validated codes of computational fluid mechanics as direct numerical simulations (DNS) have been reported for the relative simple cases of classic corona discharges [4]. For the specific case of dielectric barrier device (DBD) actuators, which we study here, efforts have been also reported recently by different researchers [1,2,5].

Corke and Post [5] derived a simplified expression for the body force distribution and implemented it in the numerical flow solver CFL3D [6] to estimate the aerodynamic coefficients involved in the control of leading-edge separation on wing sections. Likhanskii et al. [7] developed a more detailed physical model for DBD in air, and noted the computational difficulties of plasma numerical simulation over large time and spatial scales. They concluded that in general, the cell size for the rectangular grid has to be

*Corresponding author.
E-mail addresses: aleg@fi.uba.ar (A. Gronskis), gartana@fi.uba.ar (G. Artana), jorgehs@pucrs.br (J.H. Silvestrini).

0304-3886/$ - see front matter © 2007 Elsevier B.V. All rights reserved.
doi:10.1016/j.elstat.2007.06.007

chosen according to the characteristics of plasma and voltage scales and geometrical size (on the order of 10 μm); this in turn requires an extremely high number of computational points in order to perform calculations in large-scale geometries (i.e., beyond the domain which is next to the electrode configuration). The other difficulty in plasma-effects simulations is the choice of time step. Because the time step should allow for the resolution of plasma formation and sheath dynamic time (which is of the order of nanoseconds), this time scale must be several orders of magnitude smaller than the time scale over which the plasma is producing an effect on the surrounding air. Therefore, both factors render prohibitive an easy approach to detailed plasma actuation over large spatio-temporal scale using DNS. A more recent computational exploration has been conducted by Visbal et al. [3] using large-eddy simulation approaches at a Reynolds number $Re \sim 10^4$ in order to capture the effects of the local forces of the DBD device on turbulent, separated flows. Unfortunately, these researches also concluded that further work is still needed in order to construct detailed models for the spatio-temporal distribution of the plasma-induced body forces suitable for incorporation into flow simulations.

We propose here to examine the global effect produced by a DBD actuation on a cylinder wake by adding an equivalent tangential velocity to the surface of the body. From this point of view, we consider the possible analogy of the global effects produced by a DBD actuation to those from a moving surface. We concentrate our analysis on the case of disposing actuators on the surface of a cylinder arranged in such a way that their action can be imitated by the rotation of a cylinder about its axis. The present work aims to test the adequacy of this approach and to find the correspondence between the cylinder rotational parameter and the intensity of the EHD actuation. To this end, DNS of flow past a rotating cylinder placed in a uniform stream were performed for various tangential velocities using the virtual boundary technique to model the moving surface. The mean-velocity fields obtained in this way were compared with those obtained from particle image velocimetry (PIV) measurements of a DBD plasma-actuated flow.

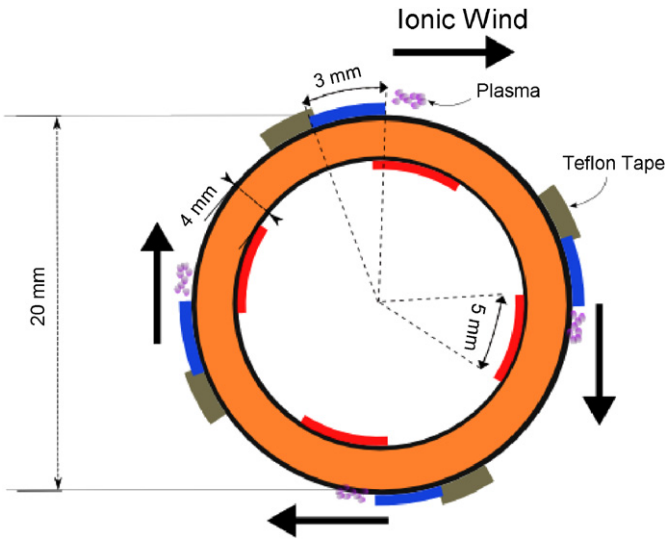

Fig. 1. Schematic of the EHD actuator.

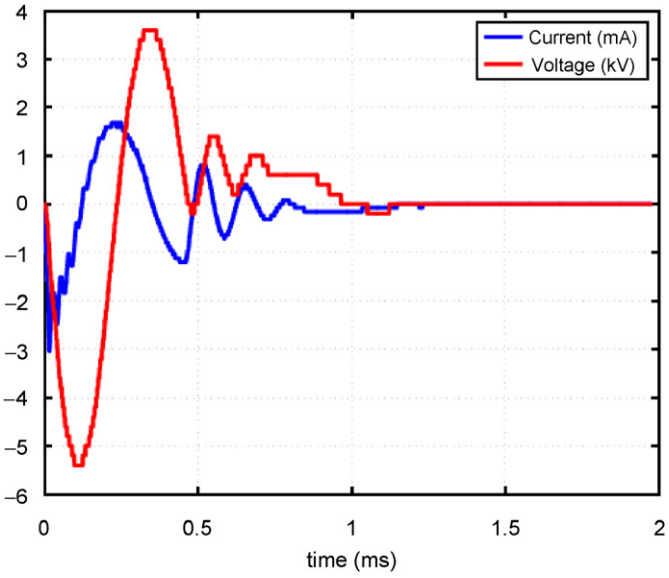

Fig. 2. Calculated current and applied voltage as a function of time.

2. Experimental setup

2.1. Wind tunnel and cylinder

The experimental configuration used in this work consisted of a flow imposed around a circular cylinder at low Reynolds number: $Re = 125$. The velocity field measurements were undertaken with the cylinder placed in a closed loop wind tunnel with an 18-cm × 18-cm test section. The EHD actuators were mounted on the surface of a $D = 20$-mm diameter polymethyl methacrylate cylinder. The cylinder was a hollow tube having a 4-mm thick wall. The asymmetric DBD plasma actuator used in our configuration consisted of four pairs of flat aluminum-foil electrodes disposed in the span around the cylinder surface, as shown in Fig. 1. For each electrode pair, the electrode exposed to air was electrically stressed while the other, separated by the dielectric material, was grounded and was not in contact with the flow. The electrodes in a given pair overlapped by a small amount (of the order of 0.5–1 mm). In order to force the flow with only one active border per electrode pair, the border that forced the flow in the desired way was left nude, meanwhile the other borders that could introduce spurious forces were passivated with teflon tape. By doing this, we assured that the plasma discharge was produced only in the regions indicated in Fig. 1. The EHD forcing was produced by stressing the air-exposed

electrode with a pulse of decreasing amplitude (see Fig. 2). Actually, an underdampened, decaying RLC response was produced and the maximum voltage of this signal was regulated in such a way that only in the first cycle the electrical discharge occurred. The maximum of the peak was kept constant in our experiments, but the frequency of repetition of the pulses was varied over the range 0–1000 Hz. By undertaking this type of excitation, the plasma actuator operation ensured the following:

- Excitations were not extremely high for the Reynolds number in which the DNS code was validated and
- Almost "steady" excitations were produced, as the input driving frequency was well above the fluid response frequency (taking into account a Strouhal number $St \sim 0.2$, the characteristic length $D = 0.2$ m, and the vortex shedding frequency of about 1 Hz).

The measured relationship between excitation frequencies and associated electrical power are shown in Fig. 3.

2.2. Velocity field measurements of a DBD actuated cylinder wake flow

The velocity fields of DBD-actuated flows have been measured using a PIV technique. These experiments were conducted using a camera having a resolution of 640×420 pixels and 1/100 s of inter-frame intervals. A green, 150-mW laser and a rotating polyhedric mirror were used to provide illumination of the test section.

The algorithms used in this work belong to GPIV software [8] which is under GNU General Public License. We have considered for our images a two-step grid refinement; hence the final interrogation size is 16×16 pixels with 50% overlap.

The time resolution was suitable to recover the flow dynamics, and the vortex shedding frequencies were much lower than the acquisition frequency.

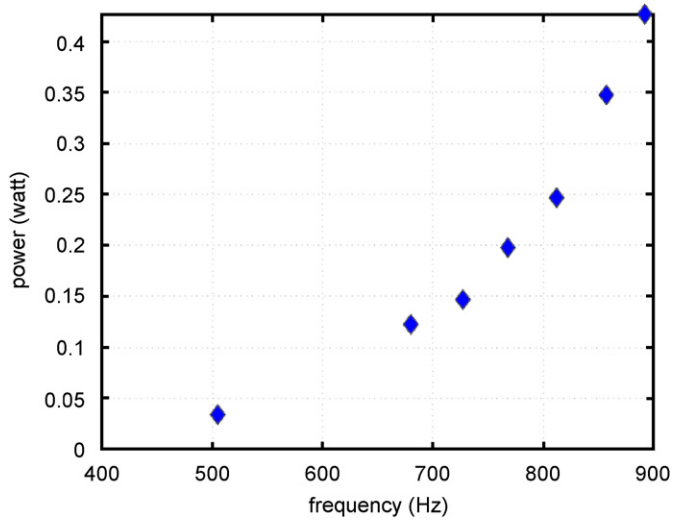

Fig. 3. Dependence of the actuator power as a function of the forcing frequency.

3. Numerical simulation of a rotating cylinder

3.1. General characteristics of the simulation code

The Incompact3d code [9–13] was used to perform the DNS studies under the assumption of two-dimensional flow. This code solves the continuity and momentum equations which are discretized using a finite-difference method on a uniform Cartesian grid.

Spatial discretization is performed with a sixth-order, compact-centered, finite difference scheme, while temporal discretization is performed using a third-order low-storage Runge–Kutta method. The boundary condition on the cylinder surface is imposed using the virtual boundary technique.

3.2. Governing equations

Mass and momentum conservation principles are represented by the Navier–Stokes equations, which have the following form for an incompressible fluid

$$\vec{\nabla} \cdot \vec{u} = 0, \tag{1}$$

$$\frac{\partial \vec{u}}{\partial t} = -\vec{\nabla} p - \vec{\omega} \times \vec{u} + \nu \nabla^2 \vec{u} + \vec{f}, \tag{2}$$

where ν is the kinematic viscosity, $p(\vec{x}, t)$ the dynamic pressure field ($P + \frac{1}{2}\rho \vec{u}^2$), $\vec{u}(\vec{x}, t)$ the velocity field and $\vec{\omega}(\vec{x}, t)$ the vorticity field ($\vec{\nabla} \times \vec{u}$). The external volumetric force field $\vec{f}(\vec{x}, t)$ is used here to impose the boundary condition on the cylinder surface.

3.3. Boundary conditions and parameters

Fig. 4 shows a schematic view of the boundary conditions over the inflow, lateral, and outflow regions of the domain. The rotation of the cylinder about its axis in the counterclockwise direction is controlled by specifying

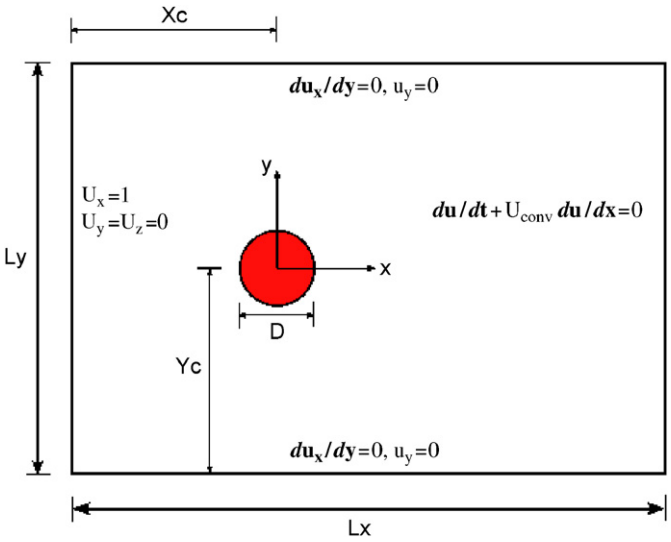

Fig. 4. Schematic of the boundary conditions.

the velocity at the surface boundary points as

$$\vec{v} = (u_x^b, u_y^b) = (-v_t \sin\theta,\ v_t \cos\theta), \tag{3}$$

$$\theta = \operatorname{arc\,tg}\left(\frac{y_b}{x_b}\right), \tag{4}$$

where $v_t = \alpha U_\infty$ is the tangential velocity of the cylinder and (x_b, y_b) are the coordinates of the boundary points of the cylinder with respect to its axis.

The simulations were performed using 685×433 grid points in the x and y directions, respectively. The domain size was $L_x = 19D$, $L_y = 12D$, and the cylinder center was located at $X_c = 8D$, $Y_c = 6D$. The grid resolution was 36 points per diameter. These parameters were considered based on the previous validation attained for the case $Re = 200$ [9,13]. A typical simulated velocity field of the undisturbed cylinder wake flow is shown in Fig. 5.

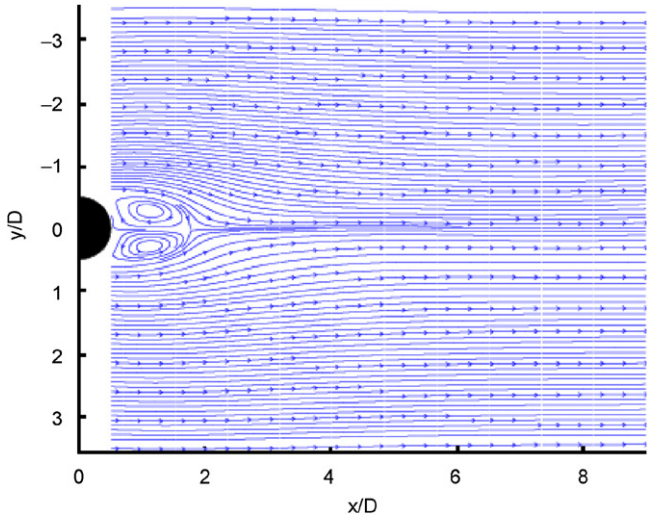

Fig. 5. Time-averaged streamlines of the undisturbed cylinder wake flow from DNS simulation, $Re = 125$.

4. Coupling mechanical rotation and EHD action

The set of EHD actuators were disposed with an aim to introduce modifications on the flow similar to a cylinder rotation. In flow around cylinders, the usual comparison between experiments and simulations is performed using the Strouhal number. However, in our analysis, this coefficient is not convenient for estimating the analogy between EHD forcing and cylinder rotation, as it is not sensitive enough to discriminate different intensities of rotation [14]. Further analysis was required and for this reason we compare the PIV results from the EHD experiments with the data obtained from simulations. We perform this by undertaking a projection based on an inner product. Assuming that our flows confined in a region Ω can be represented in Hilbert space H, the product (u, v) between two elements of H is defined as

$$(u, v) = \int_\Omega u(x)v(x)\,dx. \tag{5}$$

We propose to identify each flow by its mean flow field $\bar{u}$. Therefore, from DNS simulation we construct a function ensemble Γ with each mean flow field $\bar{u}_j$ corresponding to each value of the parameter α_j. Every element of Γ has a norm equal to unity such that $\|\bar{u}_j\| = (\bar{u}_j, \bar{u}_j)^{1/2} = 1$.

With the PIV data we construct the mean flow fields $\bar{u}_i$ corresponding to each value of DBD frequency actuation f_i. According to Fig. 3, it is possible to associate f_i with the corresponding non-dimensional electrical power W_i. The actuator power is normalized by $\rho U_\infty^3 DL$, where ρ is the fluid density and L the span of the cylinder.

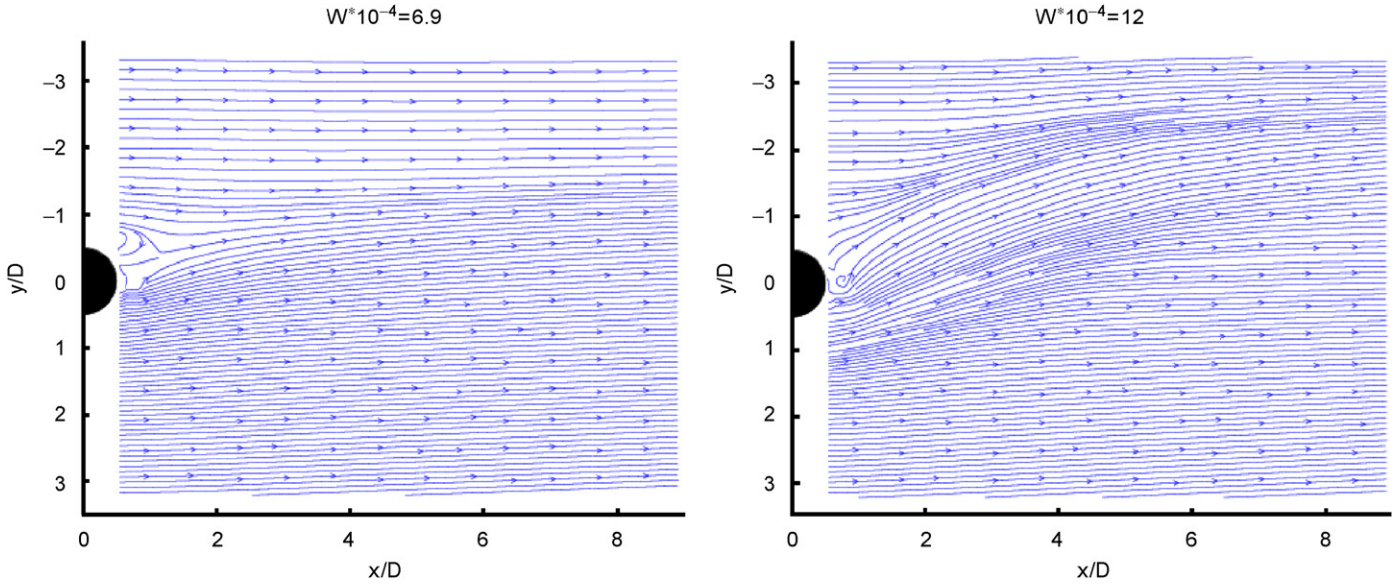

Fig. 6. Experimental time-averaged streamlines from PIV measures of DBD plasma actuator flow at various frequencies of pulse repetition.

The projection of these fields over each element of Γ gives us a parameter $p_{ij} = (\bar{u}_i, \bar{u}_j)$ which allows us to compare EHD and mechanical actuation. We established the correspondence when p_{ij} reached its maximum value.

5. Results and discussion

In our experiments, depending on the frequencies of pulse repetition, the flow could either achieve a steady state or reach a temporally periodic regime. Representations of typical experimental time-averaged streamlines are shown in Fig. 6.

The usual Karman vortex street was observed for low values of power of actuation. In these situations vortices are shed alternately and the flow achieved a temporally periodic state. The actuation introduced an asymmetry in the strength and location of the positive and negative vortices. An increase in actuation was accompanied by an increase in the upward deflection of the wake and a reduction in its lateral width. At a non-dimensional electrical power close to 7.6×10^4 (corresponding to 0.27 W) the vortex shedding ceased and the flow achieved a steady regime. A mechanical system that rotates the same cylinder and that is described in [15] requires 0.75 W to make the flow achieve the steady regime. So, DBD actuators under the configuration and kind of excitation considered resulted in a more-efficient transforming of the electric energy to kinetic energy of the flow than the mechanical one.

For the same Reynolds of our experiments ($Re = 125$) flows contouring a cylinder with various α values between 0 and 4 were computed numerically. As rotation increases the simulations show a transition from a regime with alternate vortex shedding to another one where it disappears. As can be observed from Fig. 7, when vortex shedding ceases, the flow patterns and vortical structures of time-averaged flows from the two sources show similarities with each other.

From these similarities of pattern flows it was possible to determine the equivalent value of α for the different DBD actuations. Fig. 8 shows the result of the projection described in Section 4. Based on the projection criteria,

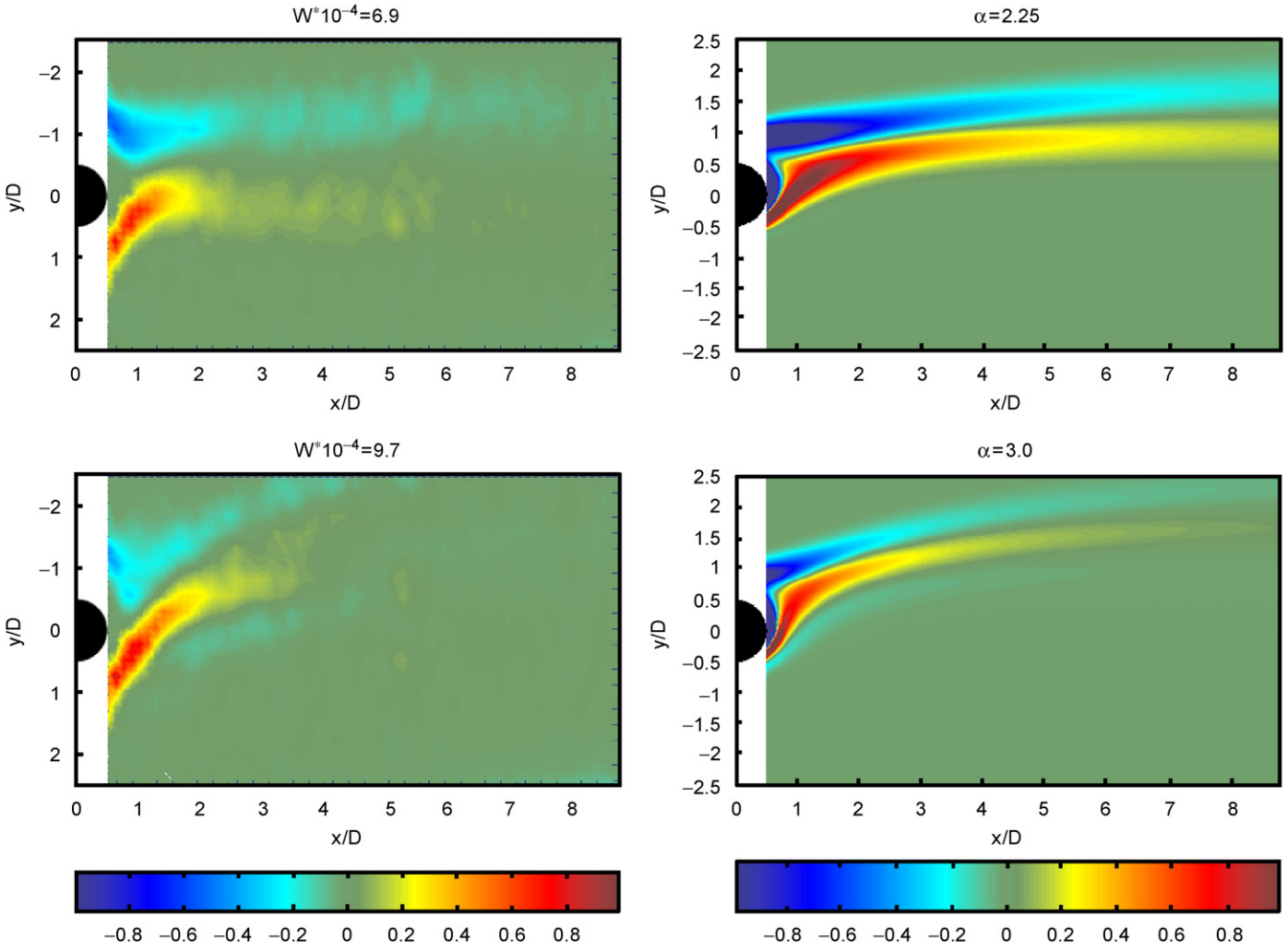

Fig. 7. Comparison of the time-averaged vorticity fields from PIV measures of DBD plasma actuator flow and those from DNS. (The vorticity is normalized with U_∞/D).

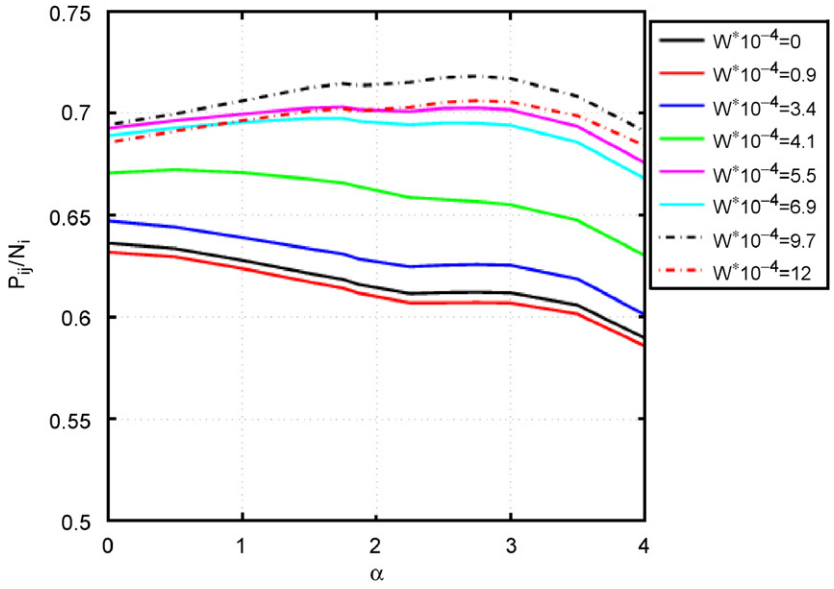

Fig. 8. Normalized projection of PIV-DBD mean fields over DNS functions ensemble Γ.

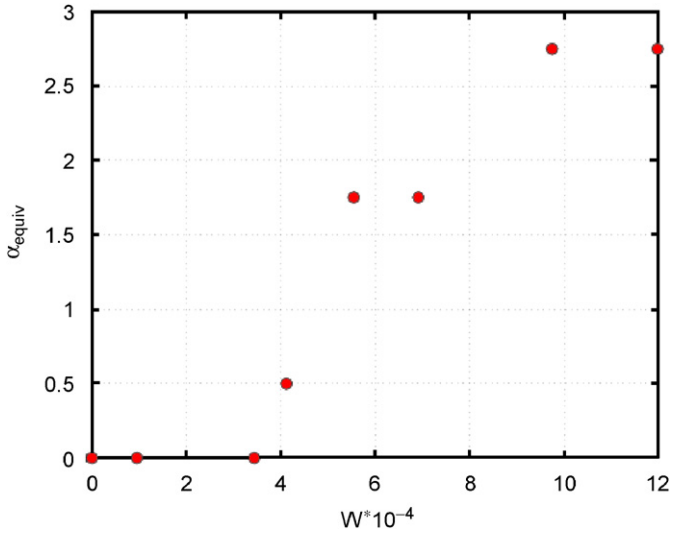

Fig. 9. Equivalent values of α for the different DBD actuations.

we could construct Fig. 9 that enables us to determine these values for the different cases analyzed. The analysis of these figures reveals that stronger correlations could be achieved for the steady cases and that the value of the equivalent rotation parameter increases in a way quite similar to that of the electrical power of the discharge.

6. Conclusion

In this work, we show that a correspondence between the wake modifications from an electro-hydrodynamic (EHD) actuation and those obtained from a moving body surface is possible.

The mean structural features of the dielectric barrier discharge (DBD) actuated wake flows observed experimentally through particle image velocimetry (PIV) measures are satisfactorily recovered numerically through direct numerical simulation (DNS) when DBD actuation is represented as a tangential velocity at the wall. The problem can then be reduced to the analysis of the flow past a rotating cylinder.

Further investigations are necessary in order to improve this correspondence by refinements on numerical simulations. The correspondence has to be validated in other situations also, like those in which actuation does not involve the whole surface of the body considered. Another important remaining issue is the analysis of the incidence of three-dimensional effects that may be present in the wake dynamics in other regimes and were not considered here.

References

[1] J.P. Boeuf, L.C. Pitchford, Electrohydrodynamic force and aerodynamic flow acceleration in surface dielectric barrier discharge, J. Appl. Phys. 97 (2005) 103307.
[2] G.I. Font, W.L. Morgan, Plasma discharges in atmospheric pressure oxygen for boundary layer separation control, AIAA Paper 4632, 2005.
[3] M.R. Visbal, D.V. Gaitonde, S. Roy, Control of transitional and turbulent flows using plasma-based actuators, AIAA Paper 2006-3230, 2006.
[4] A. Soldati, S. Banerjee, Turbulence modification by large-scale organized electrohydrodynamic flows, Phys. Fluids 10 (7) (1998) 1742–1750.
[5] T.C. Corke, M.L. Post, Overview of plasma flow control: concepts, optimization and applications, AIAA Paper, 2005-0563, 2005.
[6] NASA Langley Research Center, 〈http://cfl3d.larc.nasa.gov/Cfl3dv6/cfl3dv6.html〉, 2007.
[7] A.V. Likhanskii, M.N. Shneider, S.O. Macheret, R.B. Miles, Modeling of interaction between weakly ionized near-surface plasmas and gas flow, AIAA Paper 2006-1204, 2006.
[8] G. van der Graaf, GPIV software, 〈http://gpiv.sourceforge.net〉, 2007.
[9] A. Gronskis, J. D'Adamo, G. Artana, J. Silvestrini, Direct numerical simulation of flow past a rotating cylinder, in: Anais da 5a EPTT 2006-ABCM, Rio de Janeiro, Brazil, September 25–30, 2006.

[10] E. Lamballais, J. Silvestrini, Direct numerical simulation of interactions between a mixing layer and a wake around a cylinder, J. Turbul. 3 (2002) 028.
[11] J.H. Silvestrini, E. Lamballais, Direct numerical simulation of wakes with virtual cylinders, Int. J. Comput. Fluid Dynam. 16 (4) (2002) 305–314.
[12] P. Ribeiro, Desprendimento de vortices e controle em esteira de cilindros por simulacao numerica direta, Master's Thesis, Instituto de Pesquisas Hidraulicas-IPH/UFRGS, 2002.
[13] M. Vitola, Influencia de um contorno plano sobre o desprendimento de vortices ao redor de um cilindro circular, Ph.D. Thesis, Instituto de Pesquisas Hidraulicas-IPH/UFRGS, 2006.
[14] C.W. Van Atta, Hopf bifurcation in wakes behind a rotating and translating circular cylinder, Phys. Fluids 8 (1972).
[15] J. D'Adamo, Reduced order model for flow control with EHD actuators, Ph.D. Thesis, Universidad de Buenos Aires, March 2007.